



Contents lists available at ScienceDirect

Arabian Journal of Chemistry

journal homepage: www.ksu.edu.sa

Highly efficient eco-friendly drug inhibitors for Q235 steel in 1 M HCl: Experimental & theoretical study

Li Feng^{a,b,*}, Siyuan Zheng^a, Jianan Li^a, Xuemei Ma^a, Hailin Zhu^a, Zhiyong Hu^{a,*},
Yongqiang Sun^a

^a School of Chemical Engineering and Technology, North University of China, Taiyuan, 030051, China

^b Dezhou Graduate School, North University of China, Dezhou, Shandong 253034, China

ARTICLE INFO

Keywords:

Q235 steel
Corrosion inhibitor
Drug
Adsorption

ABSTRACT

The issue of environmental pollution has received considerable critical attention in recent years. It is necessary to develop the green and efficient corrosion inhibitors. In this paper, the inhibition of doxazosin mesylate (DM) and terazosin hydrochloride (TH), as green corrosion inhibitors, were explored systematically by electrochemical impedance, polarization curves, SEM, AFM and contact angle. The effect of different heterocyclic amounts on the corrosion inhibition efficiency for Q235 steel in 1 M HCl was also discussed. It was found that DM showed the better performance than TH, with the best corrosion inhibition efficiency of 96.4 % at 1 mg/L. The FTIR and XPS analysis of the corroded Q235 steel surface revealed that the two drugs formed adsorption films on the steel surface and the types of adsorption were chemical and physical adsorption. Finally, the mechanism of the two drugs was analyzed in detail by isothermal adsorption simulations, quantum chemical calculations and molecular dynamics simulations.

1. Introduction

All the time, Q235 steel is one of the most important metal materials in human daily production, playing an irreplaceable role in ship-building, automobile manufacturing, infrastructure construction, petrochemical industry and pipeline transportation (Xing et al., 2020, Wu et al., 2022, Dong et al., 2023). However, the characteristics of iron elements lead to its easy corrosion in service (Zheng et al., 2022, Zhu et al., 2022). These seemingly insignificant corrosion often hides a huge hidden danger (Li et al., 2021, Liu et al., 2023a, 2023b). The corrosion of metal has a serious impact on economy, safety, environment, using of new technologies and so on. At present, the main means of inhibiting metal corrosion are changing the metal structure, applying anti-corrosion coatings and adding corrosion inhibitors to the corrosive medium (Liu et al., 2019, Zhang et al., 2021a, 2021b, 2021c, Liu et al., 2022a, 2022b, 2022c, Wan et al., 2022, Qiang et al., 2023). Because of its good effect and low cost, corrosion inhibitor has become one of the important corrosion protection methods (Huang et al., 2022, Liu et al., 2023a, 2023b, Wang et al., 2023a, 2023b).

Corrosion inhibitors as the most commonly used efficient corrosion inhibitor generally contain N, O, P, S and other heteroatomic elements

containing lone pair of electrons, through the formation of coordination bonds with iron adsorbed on the surface of Q235 steel to achieve the purpose of inhibiting metal corrosion (Lin and Zuo, 2019, Zhao et al., 2019, Wu et al., 2021, Huang et al., 2023). However, organic inhibitors are volatile, poor water solubility and unfriendly to the environment (Dong et al., 2019, Zhang et al., 2020, Xiong et al., 2021, Zhang et al., 2021a, 2021b, 2021c, Wang et al., 2023a, 2023c). Therefore, it is significant to develop green and efficient environmental corrosion inhibitors (Wang et al., 2022). Currently, many medical drugs have a large number of heterocyclic structures, unsaturated bonds containing lone pairs of electrons. These drugs can be injected and taken into organisms, which makes their biological toxicity lower. Thus, these drugs have the potential to become green and efficient corrosion inhibitors (Guo et al., 2020a, 2020b, Zhang et al., 2021a, 2021b, 2021c). In recent years, many clinical drugs have been reported as corrosion inhibitors, such as phenothiazine, chloramphenicol, gentamicin, etc (Feng et al., 2020a, 2020b, 2020c, Qiang et al., 2021, Feng et al., 2023a, 2023b, Shetty et al., 2023). However, the influence of the structure of the drug on the corrosion inhibition properties has not been studied in detail due to the excessive structural differences between different clinical drugs.

Therefore, in this study, Doxazosin mesylate (DM) and Terazosin

* Corresponding authors at: School of Chemical Engineering and Technology, North University of China, Taiyuan, 030051, China (L. Feng).

E-mail addresses: fengli_nuc@163.com (L. Feng), huzhiyong@nuc.edu.cn (Z. Hu).

<https://doi.org/10.1016/j.arabjc.2023.105535>

Received 26 August 2023; Accepted 5 December 2023

Available online 13 December 2023

1878-5352/© 2023 The Authors. Published by Elsevier B.V. on behalf of King Saud University. This is an open access article under the CC BY-NC-ND license (<http://creativecommons.org/licenses/by-nc-nd/4.0/>).

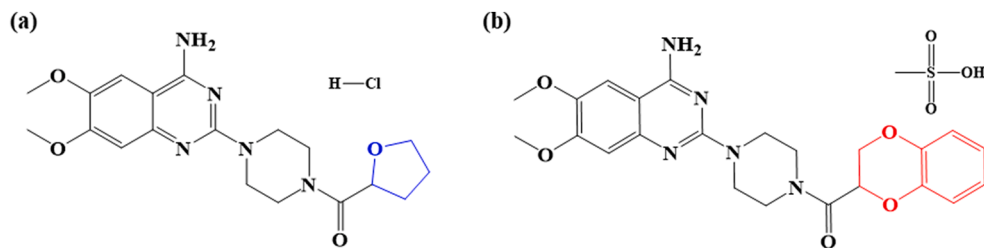


Fig. 1. The structures of Terazosin hydrochloride (TH, (a)) and Doxazosin mesylate (DM, (b)).

hydrochloride (TH) with similar structure are used to investigate the effect of different numbers of heterocycles on their corrosion inhibition properties by electrochemical polarization curves (TAFEL), electrochemical impedance spectroscopy (EIS), scanning electron microscopy (SEM), atomic force microscopy (AFM). After that, the mechanism of corrosion inhibition was explored by contact angle, FTIR (Fourier Transform Infrared Spectroscopy) and XPS (X-ray Photoelectron Spectroscopy). Finally, the isothermal equations of adsorption, quantum chemical calculations and molecular dynamics simulations were further used to analyze the corrosion inhibition mechanism of these two drugs in depth. It will provide a reference for the future research on these two drugs as corrosion inhibitors.

2. Experimental details

2.1. Materials

The clinical drugs used in this experiment were Doxazosin mesylate (DM, C₂₃H₂₅N₅O₅·CH₄O₃S, 99 %) and Terazosin hydrochloride (TH, C₁₉H₂₆ClN₅O₄, 98 %) purchased from Adamas-beta®. Hydrochloric acid (36 % ~ 38 %) was acquired from Chengdu Kolon Chemical Reagent Factory, and anhydrous ethanol (99.7 %) was bought from Tianjin Damao Chemical Reagent Factory. The chemical composition of Q235 steel sample is C:0.42 % ~ 0.50 %; Cr: ≤ 0.25 %; Mn: 0.50 % ~ 0.80 %; Ni: ≤ 0.25 %; P: ≤ 0.035 %; S: ≤ 0.035 %; Si: 0.17 % ~ 0.37 %, the balance of Fe.

2.2. Corrosion electrochemistry measurements

The electrochemical impedance spectrum and polarization curves of the two drug inhibitors were tested using the CHI 710 electrochemical workstation from Shanghai C&H. The test system uses a conventional three-electrode system, in which the reference electrode is a saturated glycerol electrode, the auxiliary electrode is a platinum electrode, and the working electrode is a Q235 steel electrode with an exposed surface of 1 cm². The working electrode surface was polished to a mirror surface using #400-#3000 water abrasive sandpaper before the test, followed by an open circuit potential method, electrochemical impedance spectrum and polarization curves test at 298 K. The test time of open circuit potential Method was 1500 s. In this time range, the change of electrode potential did not exceed 3 mV, which indicated that the system reached a steady state. Subsequently, electrochemical impedance spectrum was performed in the frequency range of 0.01–100000 Hz using a sinusoidal voltage of 5 mV. The electrochemical impedance spectrum data were fitted using ZsimpWin software. The polarization range of the polarization curve was ± 250 mV based on the open circuit potential with a scan rate of 1 mV/s.

2.3. Corrosion surface analysis (SEM, AFM and contact angle)

The Q235 steel samples were immersed in 1 M hydrochloric acid solution without and with 1 mg/L DM and TH respectively at 298 K for 24 h. The surface morphology, surface roughness and hydrophobicity were analyzed detailedly by scanning electron microscopy (SEM),

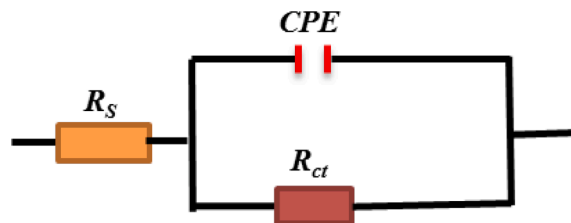


Fig. 2. The equivalent circuit fitting the electrochemical impedance data.

atomic force microscopy (AFM) and contact angle to evaluate the corrosion inhibition performance of the two drugs.

2.4. Inhibition mechanism

2.4.1. Corrosion surface chemical composition analysis

EDS (Energy Dispersive Spectroscopy), FTIR (Fourier Transform Infrared Spectroscopy) and XPS (X-ray Photoelectron Spectroscopy) tests were utilized to study the surface elemental composition, valence state and the type of functional groups after immersion and analyze the corrosion mechanism of the two drugs.

2.4.2. Thermodynamic adsorption isothermal simulation

In order to confirm the adsorption type of two drug corrosion inhibitors on the Q235 steel surface, the Langmuir, Flory-Huggins, Frun-kin and EI-Awady adsorption isotherm models were used to fit EIS and Tafel data to reveal their adsorption mechanisms on the steel surface.

2.4.3. Theoretical calculation

Quantum chemical calculations were performed using Gaussian 09 W software. And the B3LYP method of density functional theory (DFT) was applied to perform ensemble optimization and frequency calculations for the structures of two drug corrosion inhibitors using the 6311 + G (d, p) basis set. The electron cloud distribution of the highest occupied molecular orbital (HOMO) and the lowest unoccupied molecular orbital (LUMO), the energy of HOMO (E_{HOMO}), the energy of LUMO (E_{LUMO}) and ΔE -energy gap parameters were obtained.

The Forcite module of Material 7.0 software was used to investigate the molecular dynamics simulations of two drugs. Firstly, the Fe (110) crystal plane was chosen as the object of study to establish a 5 × 5 Fe cell, and then it was fixed in a box with periodic boundary conditions, after which one molecule of drug corrosion inhibitor and 491 molecules of H₂O, 9 H₃O⁺, and 9Cl⁻ were introduced to simulate experimental conditions. The COMPASS stand and NVT system were used to simulate the adsorption of corrosion inhibitors on the metal surface with a simulation step of 1 fs, a time of 1000 ps and a temperature of 298 K. Finally, the kinetic adsorption model and interaction energy ($E_{interact}$) between drug corrosion inhibitor molecules and steel surface were obtained. Fig. 1.

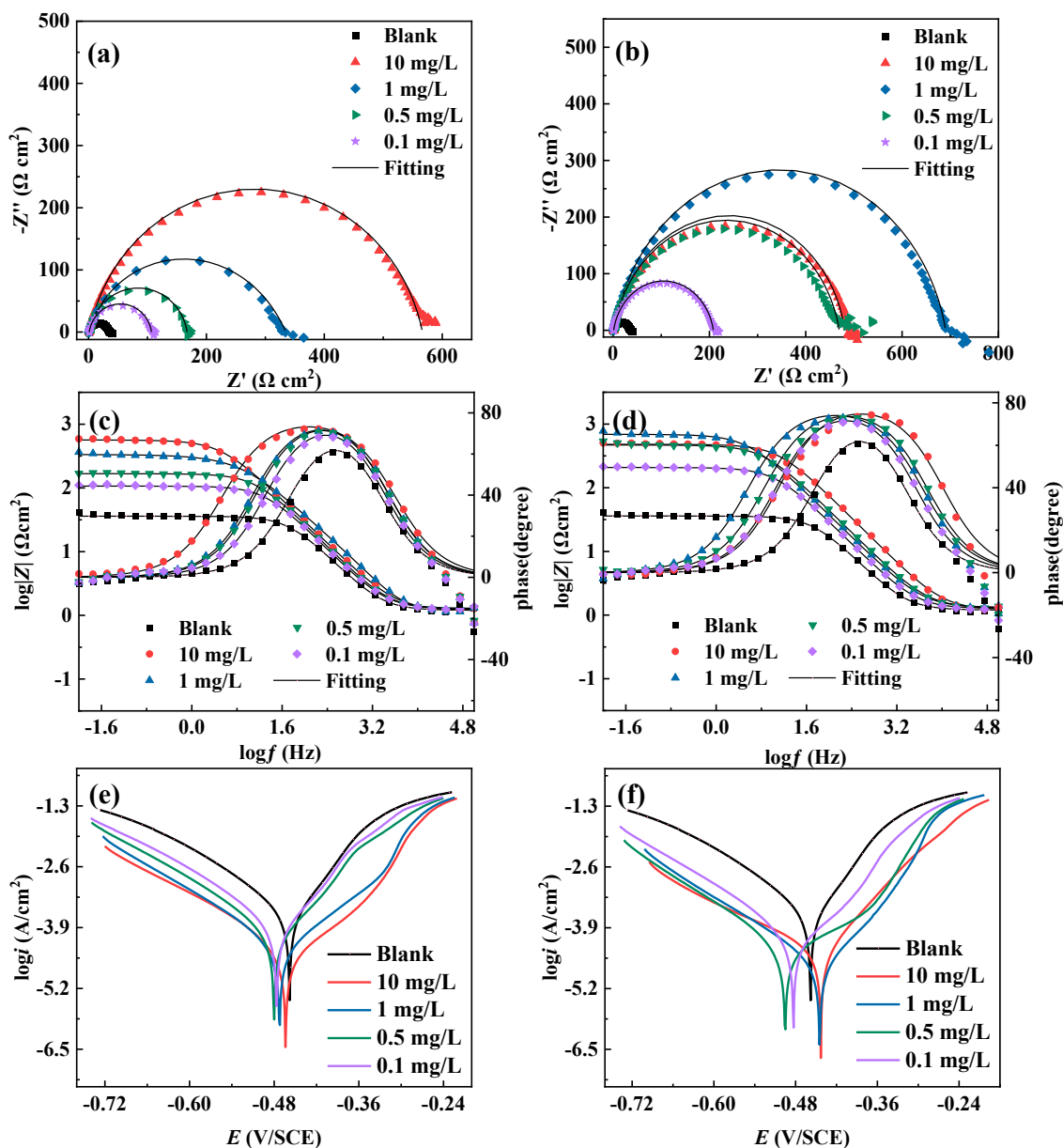


Fig. 3. The Nyquist, Bode and Tafel plots with different types and concentrations of drugs at 298 K; DM ((a), (c), (e)) and TH ((b), (d), (f)).

Table 1

The parameters for EIS measurements with different concentrations of drug corrosion inhibitors at 298 K.

	C (mg/ L)	R (Ω cm^2)	$Y_0 \times 10^5$ ($\Omega \text{ cm}^2$)	n	C_{dl} (μFcm^{-2})	R_{ct} (Ω cm^2)	η_E (%)
Blank	0	1.036	15.950	0.917	96.46	25.0	–
DM	10	1.217	4.141	0.893	26.05	479.8	94.7
	1	1.297	7.602	0.877	51.40	689.1	96.4
	0.5	1.260	8.169	0.882	52.44	468.1	94.1
	0.1	1.270	10.800	0.892	67.65	206.8	87.9
	10	1.196	10.280	0.870	63.26	565.2	95.5
TH	1	1.230	10.840	0.897	70.79	334.0	92.5
	0.5	1.252	11.090	0.900	72.53	166.0	84.9
	0.1	1.287	11.970	0.903	75.37	105.6	80.6

3. Results and discussion

3.1. Corrosion electrochemistry analysis

Fig. 2 is the equivalent circuit fitting the electrochemical impedance data. The Nyquist, bode plots and potentiodynamic polarization curves of drug inhibitors with different concentrations are shown in Fig. 3. The relevant parameters are listed in Tables 1 and 2. It can be seen that the Nyquist plots of both drug corrosion inhibitors show a semicircular shape, and this single capacitive arc of resistance indicates that the corrosion of Q235 steel in the corrosive solution is controlled by the charge transfer resistance (Feng et al., 2020a, 2020b, 2020c). Along with the increase in the concentration of the two drug corrosion inhibitors, the shape of the impedance arc is not significantly changed, which suggests that the change in the concentration of corrosion inhibitors is not caused by a change in the corrosion mechanism. Its capacitive arc of resistance first increases after decreasing, and reaches the best inhibition effect at 1 mg/L. This implies that if the concentration of DM (corrosion inhibitor) in the corrosive medium exceeds 1 mg/L, it

Table 2

The parameters for Tafel measurements with different concentrations of drug corrosion inhibitors at 298 K.

	C (mM)	E_{ocp} (mV/SCE)	E_{corr} (mV/SCE)	i_{corr} (A cm ⁻²)	β_c (mV dec ⁻¹)	β_a (mV dec ⁻¹)	η_T (%)
Blank	–	–482.9	–468.8	4.872×10^{-4}	–92.4	146.5	–
DM	10	–444.9	–444.1	3.954×10^{-5}	–64.7	160.2	91.9
	1	–452.0	–447.8	1.823×10^{-5}	–92.2	184.4	96.3
	0.5	–482.0	–494.1	4.593×10^{-5}	–93.9	80.8	90.6
	0.1	–488.3	–483.7	5.271×10^{-5}	–97.8	178.7	89.2
TH	10	–464.0	–466.8	3.180×10^{-5}	–90.7	127.8	93.5
	1	–475.0	–475.2	4.766×10^{-5}	–95.1	136.2	90.2
	0.5	–480.2	–479.4	7.435×10^{-5}	–98.9	198.5	84.7
	0.1	–477.1	–477.3	9.928×10^{-5}	–99.2	191.8	79.6

can potentially trigger an interaction where the corrosion inhibitor molecules competitively adsorb with water. As a consequence, the corrosion inhibitor molecules located outside the active zone begin to desorb, resulting in a deterioration of the corrosion inhibition

performance. For TH, the corrosion inhibition effect of gradually enhances with the increase of concentration, and the radius of capacitive arc resistance increases significantly at the concentration up to 10 mg/L compared with that at 1 mg/L, which means that the adsorption of TH is more suitable at the concentration of 10 mg/L. In addition, the above trend can also be seen through the bode plots. From the data in the Table 1, the double-layer capacitance (C_{dl}) of both drug corrosion inhibitors decreases with increasing concentration, which may be caused by the drug corrosion inhibitors occupying the active sites on the surface of Q235 steel.

Fig. 3 shows the potentiodynamic polarization curves for different concentrations of the two drug corrosion inhibitors. The inhibition effect of the cathodic branch is more obvious than that of the anodic branch at low concentrations of the two drug corrosion inhibitors. And the enhancement of the inhibition effect of the cathodic branch slows down with the gradual increase of the corrosion inhibitor concentration, while the improvement of the inhibition effect of the anodic branch becomes obvious. At the same time, the corrosion potential shifts negatively when the corrosion inhibitor is initially added, and the corrosion potential gradually moves positively as the concentration continues to increase. In the polarization curve of DM, the corrosion potential moves to the positive direction of the blank corrosion potential when the concentration reaches 1 mg/L, while the corrosion potential does not shift significantly when the concentration is increased again. It is probable that DM molecules will preferentially adsorb at the reactive sites. As the concentration of corrosion inhibitor increases, after the active

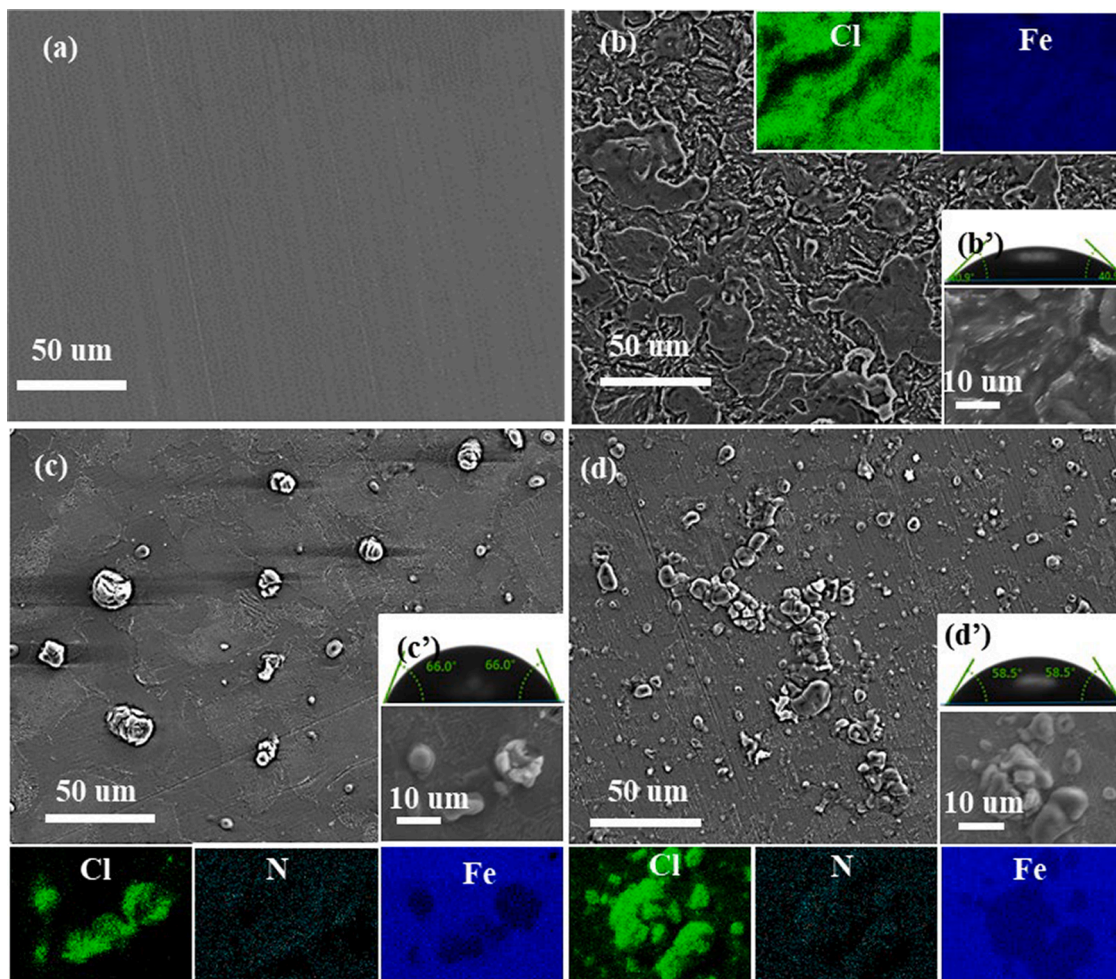


Fig. 4. SEM and contact angle pictures of samples; newly polishing (a), Blank (SEM (b) and contact angle (b')), DM (SEM (c) and contact (c')) and TH (SEM (d) and contact angle (d')).

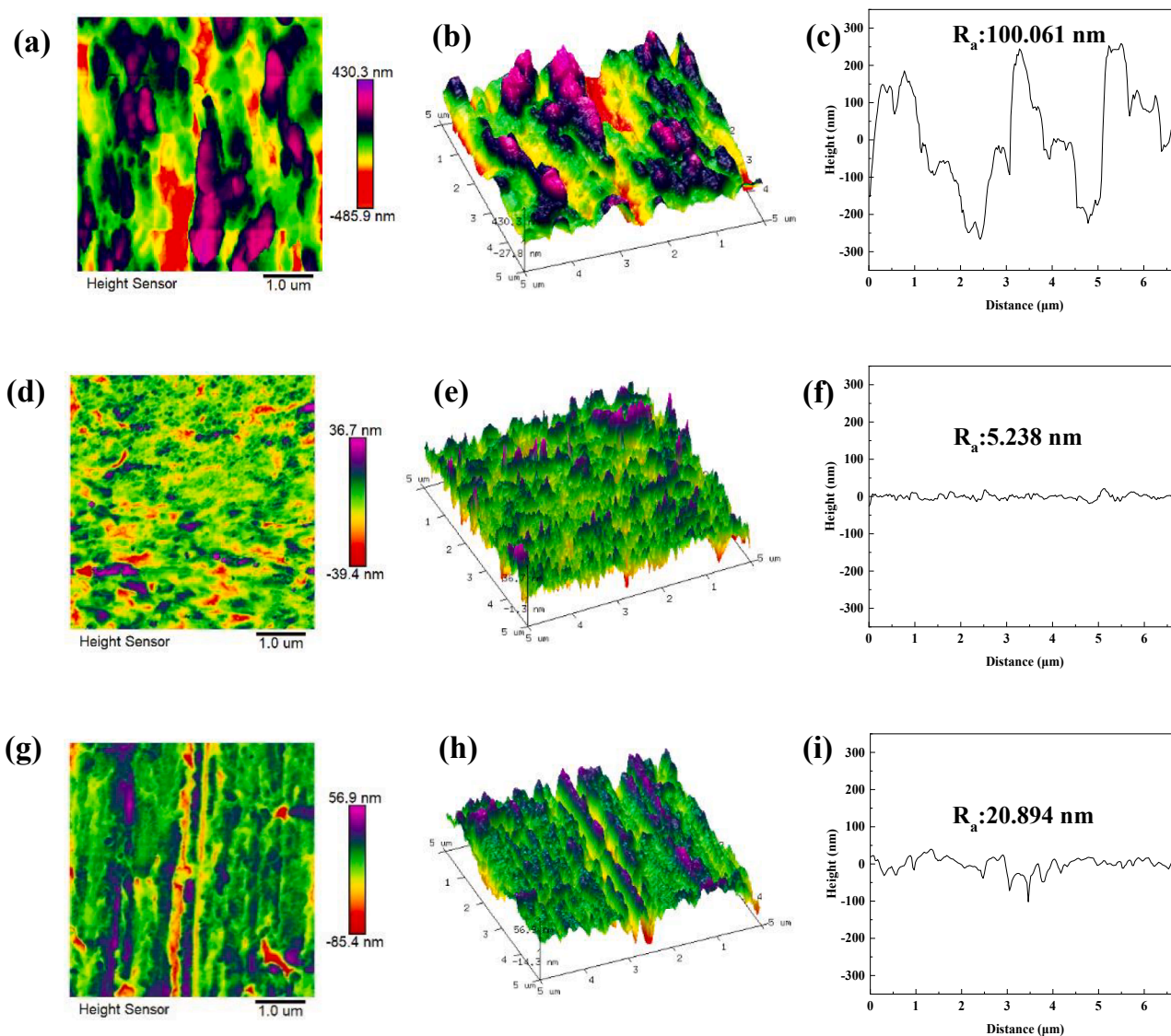


Fig. 5. AFM surface morphology images of Q235 steel samples with two drug inhibitors; (a), (b) and (c) are 2D, 3D and average roughness maps of blank; (d), (e) and (f) are 2D, 3D and average roughness maps of DM; (g), (h) and (i) are 2D, 3D and average roughness maps of TH.

adsorption centers on the metal surface are occupied, the excess corrosion inhibitor molecules start to adsorb on the inactive sites and the anodic region. From the data in the Table 2, the change of corrosion potential doesn't exceed 85 mV compared to the blank corrosion potential, which means that both drug corrosion inhibitors are mixed type corrosion inhibitors (Chen et al., 2020, Feng et al., 2023a, 2023b). The inhibition effect of DM is better than that of TH, which is mainly attributed to the fact that the number of heterocycles of DM is higher than that of TH, making it easier to adsorb to the Q235 steel surface.

3.2. SEM and contact angle test

Fig. 4 shows scanning electron microscopy (SEM) and contact angle pictures of Q235 steel samples after 24 h immersion in corrosion media with and without 1 M of two drugs corrosion inhibitors. Compared with freshly polished Q235 steel, the corrosion of the sample after immersion in hydrochloric acid solution is more serious and the surface is very rough. It is evident that the sample containing corrosion inhibitor is smoother compared to the blank, and the traces of polished metal samples can be seen. Meanwhile, the samples after immersion in the corrosive medium containing DM are smoother compared to the samples

after immersion in the corrosive medium containing TH. From the EDS, the Cl elements in the blank are widely distributed on the sample surface, and the Fe elements are relatively unevenly distributed, which should be due to the severe corrosion of the blank sample and/or a large number of corrosion products on the metal surface. While the surface of Q235 steel after immersion with corrosion inhibitors, the presence of Cl elements in the area is much smaller compared to the blank, and the distribution of Fe elements in the area where corrosion has not occurred is relatively uniform. Furthermore, the absence of N elements in the blank sample indicates that the two drug corrosion inhibitors adsorb on the surface of the metal to form a protective anti-corrosion film. The contact angle figures show that the contact angles of the DM and TH samples are about 70° and 60°, respectively, which suggests that the hydrophobicity is greatly improved compared to the blank of 30°. Also, the change in contact angle can be confirmed that the drugs corrosion inhibitor molecules form a protective film on the metal surface, changing its hydrophobic properties.

3.3. AFM analysis

Fig. 5 shows the AFM results of Q235 samples immersed in corrosion

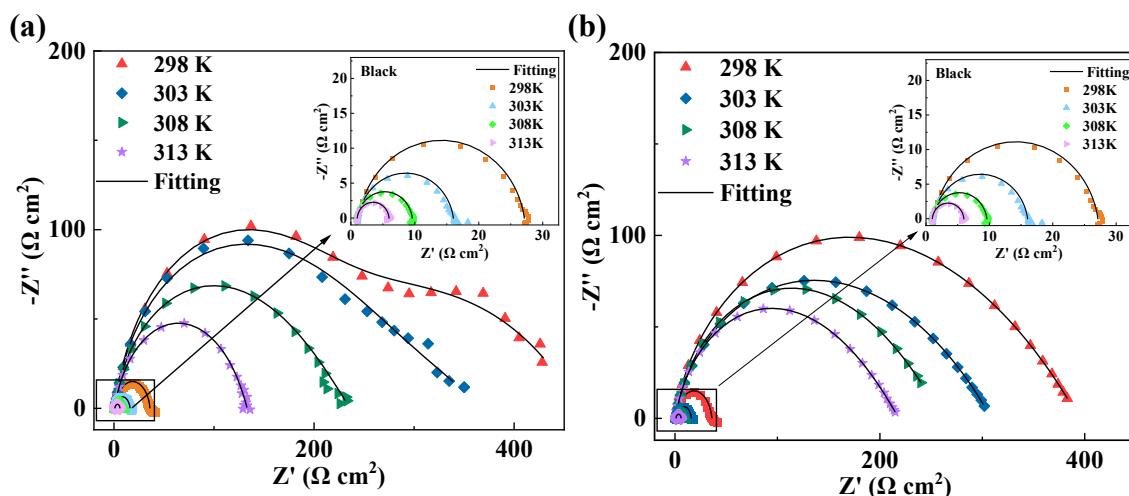


Fig. 6. Nyquist plots of Q235 steel samples in 1 M hydrochloric acid with 10 mg/L of drug corrosion inhibitors at different temperatures (DM (a), TH (b)).

Table 3

The parameters for EIS with 10 mg/L drug corrosion inhibitors at different temperature.

	T (K)	R (Ω cm²)	Y ₀ × 10 ⁻⁵ (Ω cm ⁻²)	n	C _{dl} (μFcm ⁻²)	R _{ct} (Ω cm²)	η (%)
Blank	298	1.266	15.28	0.904	85.41	25.9	–
	303	1.147	18.98	0.907	104.47	14.8	–
	308	1.015	22.52	0.917	127.77	8.5	–
	313	1.002	23.49	0.939	151.33	4.97	–
DM	298	1.258	2.91	0.981	27.90	385.7	93.3
	303	1.097	3.47	0.997	34.29	307.9	95.1
	308	1.128	3.68	0.952	29.89	259.9	96.6
	313	1.089	3.74	0.964	31.78	217.4	97.7
TH	298	1.216	8.16	0.879	49.44	382.2	93.2
	303	1.106	5.60	0.919	40.04	367.2	95.9
	308	1.159	4.45	0.949	35.68	234.9	96.3
	313	1.134	3.84	0.972	33.47	132.1	96.2

medium with and without two corrosion inhibitors for 24 h. After introducing corrosion inhibitors, the results presented in the figure clearly demonstrates a substantial reduction in the average surface roughness of the samples. For the untreated samples (blanks), the average surface roughness (R_a) is 126.0 nm. However, with the addition of corrosion inhibitors, the R_a decreases significantly to 5.1 nm for DM-treated samples and 29.2 nm for TH-treated samples. This noteworthy decrease in surface roughness indicates effective inhibition of corrosion for the metal samples in the corrosive medium with drugs.

Furthermore, the 3D plot accompanying the figures reveals that the

samples immersed in DM exhibit a smoother surface compared to those immersed in TH. This discrepancy suggests that DM has a higher efficiency in inhibiting corrosion compared to TH. The visible disparity between the surfaces of the DM and TH-treated samples further supports the notion that DM offers superior corrosion inhibition capabilities. Importantly, these Atomic Force Microscopy (AFM) results corroborate the findings of the electrochemical tests and SEM tests. Together, these complementary analyses provide comprehensive evidence for the effective corrosion inhibition achieved by the addition of corrosion inhibitors, particularly DM, resulting in a significant reduction in surface roughness.

3.4. Effect of temperature on inhibition

Fig. 6 depicts the electrochemical tests conducted on the two drug corrosion inhibitors under various temperature conditions. The impedance data are shown in Table 3. Obviously, the information in the figure shows that the corrosion inhibition efficiency of the two drug inhibitors tends to increase as the temperature rises. Among them, the corrosion inhibition efficiency of TH reaches the best (96.3 %) at 308 K. After that, the corrosion inhibition efficiency starts to decrease at higher temperatures. In Table 3, with the increase of temperature, the charge transfer resistances of the blank group and two drug inhibitors gradually decrease, but the rate of decrease for the drug corrosion inhibitors is significantly smaller than that of the blank control group, which leads to the increase of corrosion inhibition efficiency. The C_{dl} of DM increases with temperature, which should probably be attributed to the decrease

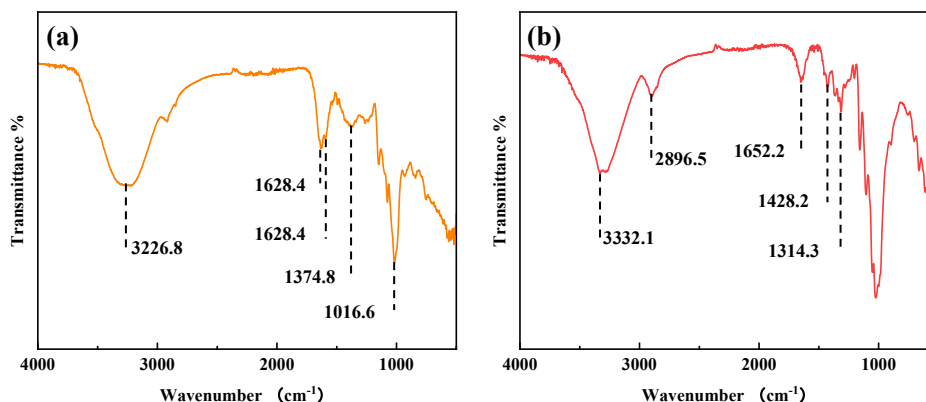


Fig. 7. FT-IR results of Q235 steel samples treated with two drug inhibitors (DM (a); TH (b)).

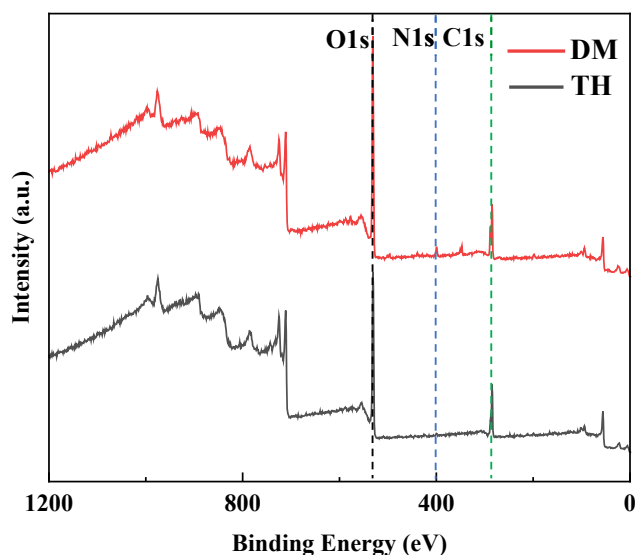


Fig. 8. The XPS survey of Q235 steel treated with DM and TH.

in the ability of DM molecules to occupy active sites on the surface of Q235 steel. For TH, the C_{dl} shows a decreasing trend with increasing temperature, which means that the increase of temperature makes the TH molecules occupy more active sites on the surface of Q235 steel. The upsurge in corrosion inhibition efficiency with the rise in temperature

can likely be attributed to the increased mobility of the corrosion inhibitor molecules in solution. The accelerated movement of these drug corrosion inhibitors facilitates the formation of a protective film on the surface of Q235 steel. Consequently, the higher temperature promotes the efficacy of the corrosion inhibition process by facilitating the formation of a more effective protective film on the Q235 steel surface.

3.5. FT-IR analysis

Fig. 7 shows the FT-IR of the Q235 sample after 12 h immersion in the corrosion medium containing the corrosion inhibitors. As shown in the figure, the Q235 steel surface treated with DM produces peaks at 3226.87 cm^{-1} for $=C-H$ stretching vibration, 1628.41 cm^{-1} for $C=N$ stretching vibration, 1589.08 cm^{-1} for benzene ring skeleton vibration, 1374.58 cm^{-1} for in-plane bending vibration characteristic of $-CH_3$, and 1016.63 cm^{-1} for $C-N$ stretching vibration (Chen et al., 2019, Zheng et al., 2023). The metal surface treated with TH has characteristic peaks at 3332.13 cm^{-1} for $N-H$ stretching vibration, 2896.52 cm^{-1} for $C-H$ stretching vibration, 1652.28 cm^{-1} for $C=O$ stretching vibration, 1428.21 cm^{-1} for skeletal vibration of the benzene ring, 1314.39 cm^{-1} for a characteristic peak of tetrahydrofuran and 1203.36 cm^{-1} represents the absorption peak of aromatic ether $C-O-C$ (Feng et al., 2018). These characteristic peaks correspond to the FTIR characteristic peaks of TH. The FTIR findings indicate that the application of two corrosion inhibitors, acting as drugs, resulted in the formation of a protective film on the surface of Q235 steel. This film altered the chemical characteristics of the Q235 steel surface, thereby effectively preventing direct contact between the corrosive medium and the Q235 steel substrate.

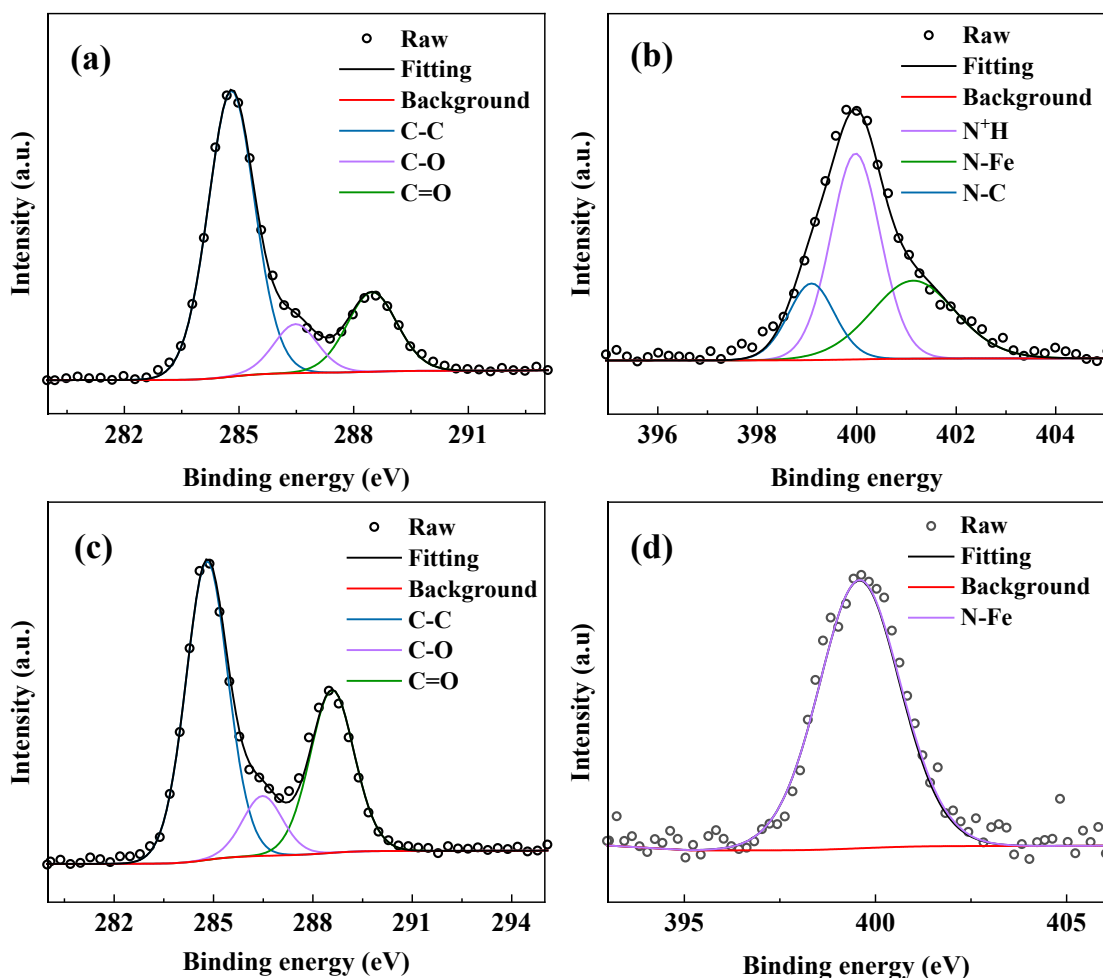


Fig. 9. The XPS high-resolution spectra of Q235 steel samples treated with two drug inhibitors (C1s (a) and N1s (b) for DM; C1s (c) and N1s (d) for TH).

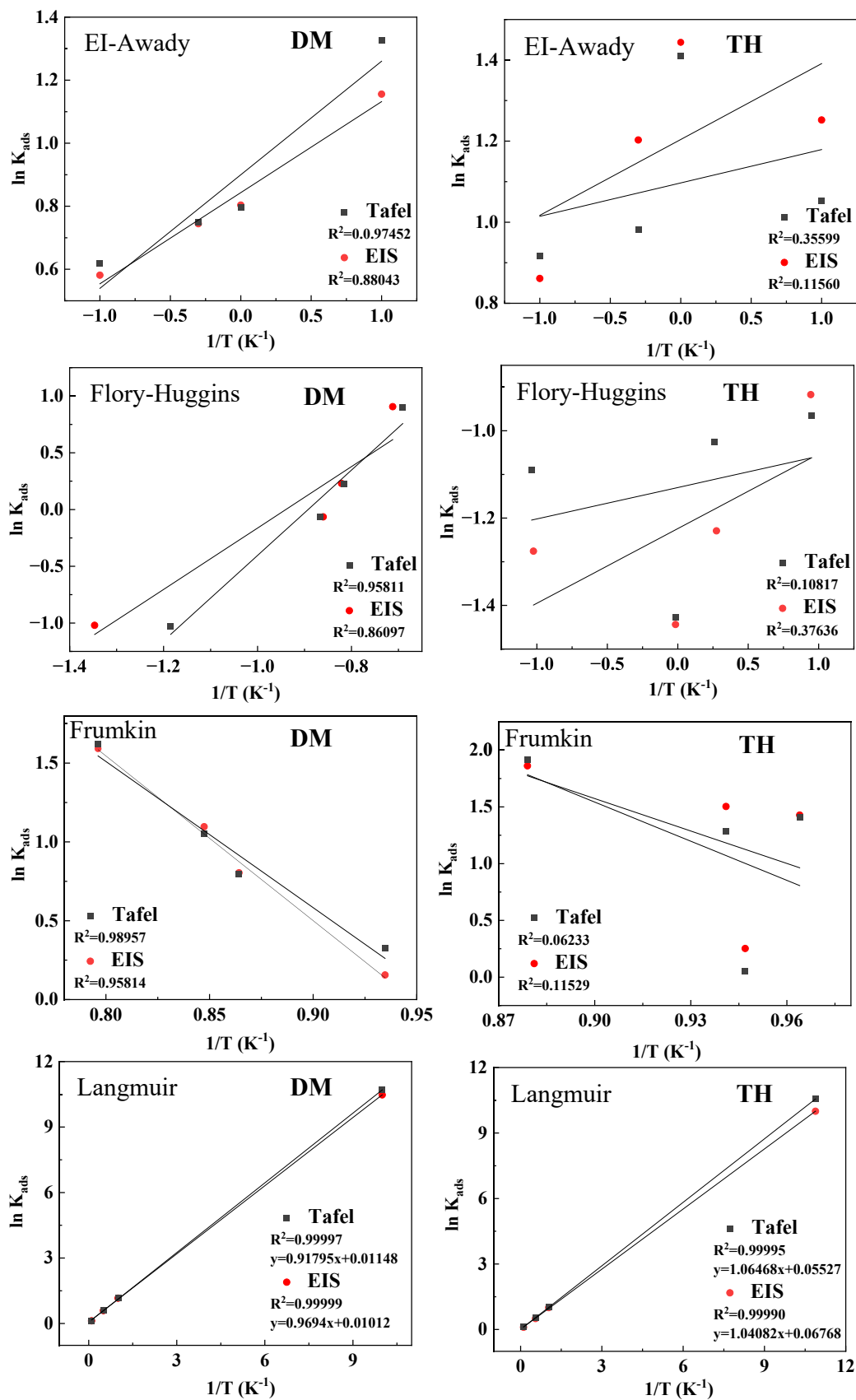


Fig. 10. Results of the EI-Awady, Flory-Huggins, Frumkin and Langmuir fittings of DM and TH.

Table 4

The relevant Langmuir adsorption isotherm parameters of DM and TH on Q235 steel surface in 1 M HCl solution at 298 K.

	K_{ads} (L/mol)	ΔG_{ads} (kJ mol ⁻¹)	ΔH_{ads} (kJ mol ⁻¹)	ΔS_{ads} (J K ⁻¹ mol ⁻¹)
DM	10.61×10^3	-38.98	-7.63	14.56
TH	10.13×10^3	-43.85	-8.85	14.93

3.6. XPS analysis

Fig. 8 displays the XPS survey spectra of Q235 samples that are immersed in a corrosive medium containing two corrosion inhibitors drugs. On the surface of the Q235 steel treated with these inhibitors, the presence of N element is detected. Additionally, there is an observable decrease in the content of O and Fe elements compared to the blank sample. This observation suggests that the organic molecules form a protective film on the surface of the Q235 steel, resulting in lower exposed Fe elements and hindering their oxidation process.

Fig. 9 shows the N1s high-resolution XPS spectra of DM-treated sample, revealing three distinctive peaks at 398.30 eV, 399.60 eV, and 401.35 eV. These peaks correspond to N—C, N—Fe, and N⁺H, respectively (Guo et al., 2020a, 2020b, Liao et al., 2023). The presence of N—Fe bonds suggests that the drug corrosion inhibitor chemically adsorbs on the Q235 steel surface. The presence of N⁺H indicates physical adsorption of the drug corrosion inhibitor with the surface of Q235 steel. These results suggest that the corrosion inhibitor forms a protective film on the Q235 steel surface through both chemical adsorption and physical adsorption, effectively slowing down metal corrosion. In contrast, the surface of TH-treated sample exhibits a single characteristic peak at 399.6 eV for the N-Fe, indicating that the N in drug TH can adsorb chemically on the Q235 steel surface by Fe and N elements (Shao et al., 2022).

In addition, the high-resolution XPS spectra of C1s show that both DM and TH produce three characteristic peaks at 288.5 eV, 286.5 eV and 284.8 eV, corresponding to C=O, C—O and C—C, respectively, which may be caused by the adsorption of the drug corrosion inhibitors on the Q235 steel surface (Feng et al., 2019a, 2019b). The detection of these bonds also indicates the formation of adsorption films on the surface of the Q235 steel by the two drug corrosion inhibitors, thus changing its

chemical properties.

3.7. Isothermal adsorption simulation

To further investigate the adsorption behavior of two drug inhibitors on the surface of Q235 steel, Langmuir, Flory-Huggins, Frunkin, and El-Awady models are utilized. The simulation results indicate that the Langmuir adsorption model best approximates the adsorption behavior of the two inhibitors. It can be observed from Fig. 10 that the R² values obtained by fitting the Langmuir model are closest to 1, suggesting that the two inhibitors can only adsorb in a monolayer on the surface of Q235 steel. The relevant Langmuir adsorption isotherm parameters of DM and TH on the Q235 steel surface in 1 M HCl solution at 298 K are presented in Table 4. According to data from K_{ads} , the molar adsorption constant (DM: 10.61×10^3 L mol⁻¹) is greater than that of TH (10.13×10^3 L mol⁻¹). This indicates that DM exhibits higher affinity for adsorption onto the surface of Q235 steel compared to TH. For DM, the value of ΔG_{ads} is -38.98 kJ/mol. Its absolute value falls between 20 kJ/mol and 40 kJ/mol, suggesting that the adsorption of DM involves a combination of chemisorption and physical adsorption processes (Wang et al., 2021a, 2021b). On the other hand, TH has a ΔG_{ads} value of 43.85 kJ/mol, with an absolute value greater than 40 kJ/mol. This indicates that the adsorption of TH on Q235 steel is mainly driven by chemical adsorption. Moreover, it is noteworthy that both DM and TH display negative values of ΔH_{ads} , indicating that the adsorption of these two drugs onto the surface of Q235 steel releases heat. This observation indicates that the adsorption process is exothermic in nature.

3.8. Quantum chemistry calculation

Fig. 11 shows the geometrically optimized structures and molecular orbital diagrams of the two drug inhibitors to investigate the corrosion inhibition mechanism, and the relevant quantum chemical parameters can be obtained. It can be seen from the figure that the active site is mainly concentrated on the benzene ring, which presents that the active center of adsorption is on the benzene ring. By analyzing the E_{HOMO} values, DM (-5.14 eV) is higher than TH (-5.73 eV), which suggests that the DM molecule has a stronger electron-donating ability, making it easier to adsorb to the surface of Q235 steel compared to terazosin hydrochloride (Fu et al., 2019, Liu et al., 2022a, 2022b, 2022c).

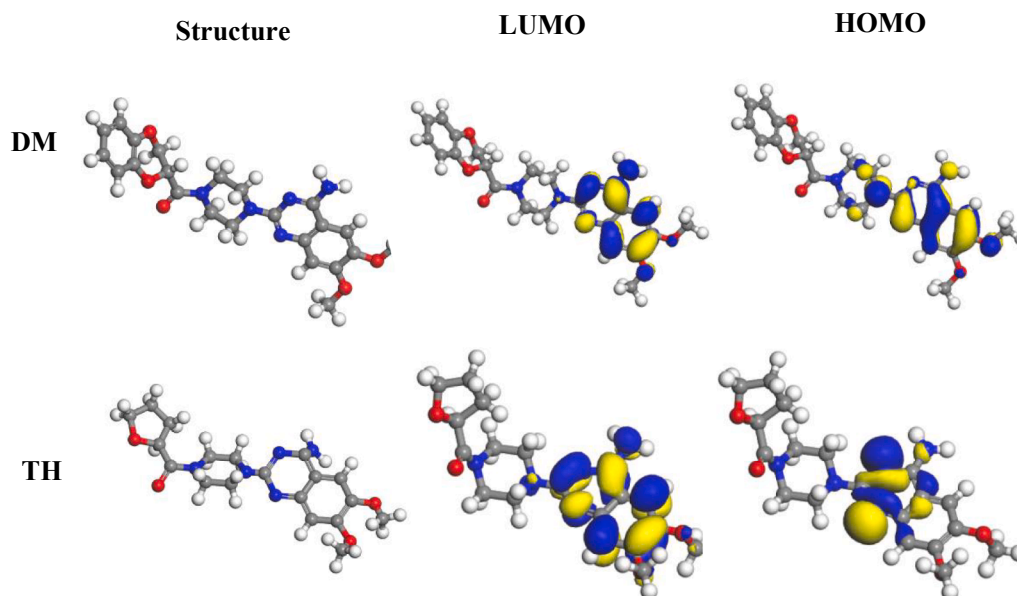


Fig. 11. Molecular frontier orbital diagram of DM and TH molecular.

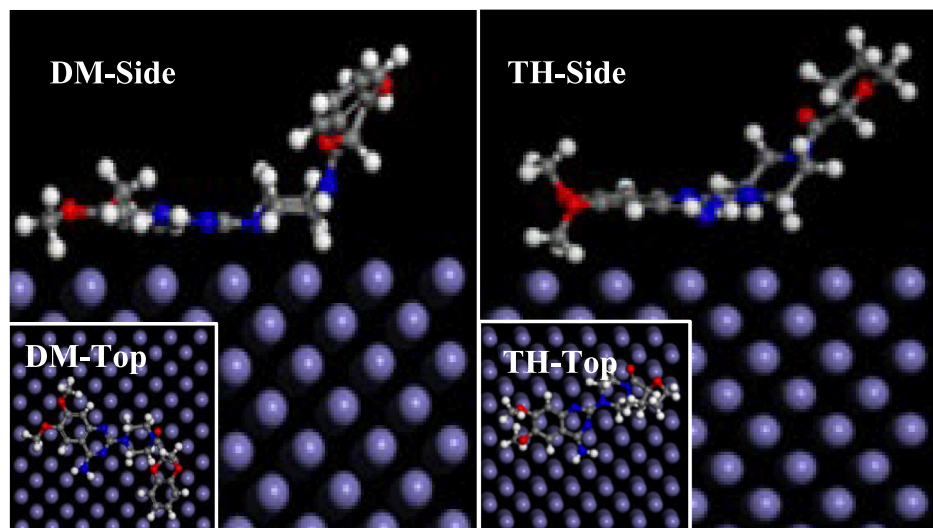


Fig. 12. Side and top views of molecular dynamics adsorption simulations of two drug corrosion inhibitors on Q235 steel surface.

Additionally, molecules with lower energy gap values (ΔE) exhibit higher reactivity and are more prone to adsorption on the metal surface. In this regard, DM ($\Delta E = 2.86$ eV) has a smaller energy gap compared to TH ($\Delta E = 4.62$ eV) (Feng et al., 2020a, 2020b, 2020c). Furthermore, the dipole moment (μ) confirms that DM ($\mu = 1.03$ eV) possesses a higher corrosion inhibition ability than TH ($\mu = 0.09$ eV) (Wang et al., 2021a, 2021b, Liu et al., 2022a, 2022b, 2022c). In summary, DM, with a greater number of heterocycles, demonstrates superior corrosion inhibition effectiveness. This conclusion aligns with above findings on corrosion inhibition efficiency.

3.9. Molecular dynamics simulation

The top and side views of the adsorption simulations of the two drug corrosion inhibitors are represented in Fig. 12. The entire benzene ring region is observed to be adsorbed onto the Q235 steel surface, confirming the findings from the quantum chemical calculations. In addition, the calculated binding energies (E_{binding} , E_{binding} is numerically equal to the absolute value of E_{interact}) of the two drug inhibitors are $320.798 \text{ kJ mol}^{-1}$ for DM and $231.283 \text{ kJ mol}^{-1}$ for TH, respectively, where the higher binding energy indicates that the target molecules have a stronger tendency to adsorb onto the Q235 steel surface, performing better inhibition efficiency (Feng et al., 2019a, 2019b). Therefore, the molecular dynamics results also support the higher corrosion inhibition properties of DM compared to TH, which is consistent with previous experimental findings.

4. Conclusion

In this study, two drugs (doxazosin mesylate (DM) and terazosin hydrochloride (TH)) with different numbers of heterocycles were systematically investigated as corrosion inhibitors for Q235 steel. Guidance is provided for the disposal of drugs as corrosion inhibitors. The following conclusions were drawn from the analytical arguments.

- (1) The electrochemistry, SEM, and AFM tests showed that both drugs exhibited high inhibition effects as corrosion inhibitors. And the more the number of heterocycles in the drug molecules, the better the corrosion inhibition efficiency.
- (2) The corrosion inhibition efficiency of two drugs increased when the temperature increased, and they could effectively protect Q235 steel from corrosion in corrosive media at temperatures of 298 K–313 K.

- (3) By FTIR and XPS, two inhibitors can adsorb onto the Q235 steel surface, and the adsorption modes were chemical and physical adsorption.
- (4) The isothermal adsorption simulations showed that both drug corrosion inhibitors conformed to the Langmuir adsorption isotherm model. It indicates that the two drug corrosion inhibitors are single molecular layer adsorption.
- (5) Quantum chemical calculations and molecular dynamics simulations showed that DM molecules with a high number of heterocycles have lower energy gap values and higher binding energies, which make them easier to adsorb on metal surfaces compared to TH molecules with a lower number of heterocycles.

Declaration of competing interest

The authors declare that they have no known competing financial interests or personal relationships that could have appeared to influence the work reported in this paper.

Acknowledgement

The authors appreciate financial support from the Natural Science Foundation of Shanxi Province (No. 20210302124337, 202103021224207), the Research Project Supported by Shanxi Scholarship Council of China (No. 2022-137) and Open Project Program of the Shanxi Key Laboratory of Advanced Carbon Materials (No. 2022C80305).

References

- Chen, S., Chen, S., Li, W., 2019. Corrosion inhibition effect of a new quinoline derivative on Q235 steel in H_2SO_4 solution. *Int. J. Electrochem. Sci.* 14, 11419–11428. <https://doi.org/10.20964/2019.12.36>.
- Chen, S., Zhao, H., Chen, S., et al., 2020. Camphor leaves extract as a neoteric and environment friendly inhibitor for Q235 steel in HCl medium: combining experimental and theoretical researches. *J. Mol. Liq.* 312 <https://doi.org/10.1016/j.molliq.2020.113433>.
- Dong, Y., Li, M., Zhang, Y., et al., 2023. Cerium dioxide modified with fumaric acid as corrosion inhibitor for epoxy coatings on Q235. *Anti-Corros. Methods Mater.* 70, 59–68. <https://doi.org/10.1108/acmm-10-2022-2708>.
- Dong, Q., Zhang, G., Zhang, W., et al., 2019. Experimental and theoretical analysis of Quinoline diquaternary ammonium salt as corrosion inhibitor. *Chem. J. Chin. Univ.-Chin.* 40, 2195–2204. <https://doi.org/10.7503/cjcu20190181>.
- Feng, L., Zhang, S., Qiang, Y., et al., 2018. The synergistic corrosion inhibition study of different chain lengths ionic liquids as green inhibitors for X70 steel in acidic medium. *Mater. Chem. Phys.* 215, 229–241. <https://doi.org/10.1016/j.matchemphys.2018.04.054>.

- Feng, L., Zhang, S., Lu, Y., et al., 2019a. Synergistic corrosion inhibition effect of thiazolyl-based ionic liquids between anions and cations for copper in HCl solution. *Appl. Surf. Sci.* 483, 901–911. <https://doi.org/10.1016/j.apsusc.2019.03.299>.
- Feng, L., Zhang, S., Xu, Y., et al., 2019b. The electron donating effect of novel pyrazolopyrimidine inhibitors on anticorrosion of Q235 steel in pickling solution. *J. Mol. Liq.* 286 <https://doi.org/10.1016/j.molliq.2019.110893>.
- Feng, L., Ren, X., Feng, Y., et al., 2020a. Self-assembly of new O- and S-heterocycle-based protective layers for copper in acid solution. *Phys. Chem. Chem. Phys.* 22, 4592–4601. <https://doi.org/10.1039/c9cp06910k>.
- Feng, L., Zhang, S., Feng, Y., et al., 2020b. Self-aggregate nanoscale copolymer of new synthesized compounds efficiently protecting copper corrosion in sulfuric acid solution. *Chem. Eng. J.* 394 <https://doi.org/10.1016/j.cej.2020.124909>.
- Feng, L., Zhang, S., Tao, B., et al., 2020c. Two novel drugs as bio-functional inhibitors for copper performing excellent anticorrosion and antibacterial properties. *Colloids Surf. B Biointerfaces.* 190, 110898 <https://doi.org/10.1016/j.colsurfb.2020.110898>.
- Feng, L., Zhang, S., Zhou, Y., et al., 2023a. Expired glucosamine drugs as green corrosion inhibitors for carbon steel in H₂SO₄ solution and synergistic effect of glucosamine molecules with iodide ions: combined experimental and theoretical investigations. *Crystals* 13. <https://doi.org/10.3390/cryst13020205>.
- Feng, L., Zheng, S., Zhu, H., et al., 2023b. Detection of corrosion inhibition by dithiane self-assembled monolayers (SAMs) on copper. *J. Taiwan Inst. Chem. Eng.* 142 <https://doi.org/10.1016/j.jtice.2022.104610>.
- Fu, S., Zhang, S., Xiang, Q., et al., 2019. Experimental and theoretical investigation of corrosion inhibition effect of multi-active compounds on mild steel in 1 M HCl. *Int. J. Electrochem. Sci.* 14, 6855–6873. <https://doi.org/10.20964/2019.07.77>.
- Guo, L., Tan, J., Kaya, S., et al., 2020a. Multidimensional insights into the corrosion inhibition of 3,3-dithiodipropionic acid on Q235 steel in H₂SO₄ medium: a combined experimental and in silico investigation. *J. Colloid Interface Sci.* 570, 116–124. <https://doi.org/10.1016/j.jcis.2020.03.001>.
- Guo, L., Zhang, R., Tan, B., et al., 2020b. Locust Bean Gum as a green and novel corrosion inhibitor for Q235 steel in 0.5 M H₂SO₄ medium. *J. Mol. Liq.* 310 <https://doi.org/10.1016/j.molliq.2020.113239>.
- Huang, Z., Liu, L., Lei, B., et al., 2023. A new imidazole derivative for corrosion inhibition of Q235 carbon steel in an acid environment. *Polymers* 15. <https://doi.org/10.3390/polym15112420>.
- Huang, L., Yang, K.-P., Zhao, Q., et al., 2022. Corrosion resistance and antibacterial activity of procyanidin B2 as a novel environment-friendly inhibitor for Q235 steel in 1 M HCl solution. *Bioelectrochemistry* 143. <https://doi.org/10.1016/j.bioelechem.2021.107969>.
- Li, H., Qiang, Y., Zhao, W., et al., 2021. A green Brassica oleracea L extract as a novel corrosion inhibitor for Q235 steel in two typical acid media. *Colloids Surf. A-Physicochem. Eng. Aspects* 616. <https://doi.org/10.1016/j.colsurfa.2020.126077>.
- Liao, B., Luo, Z., Wan, S., et al., 2023. Insight into the anti-corrosion performance of Acanthopanax senticosus leaf extract as eco-friendly corrosion inhibitor for carbon steel in acidic medium. *J. Ind. Eng. Chem.* 117, 238–246. <https://doi.org/10.1016/j.jiec.2022.10.010>.
- Lin, B., Zuo, Y., 2019. Corrosion inhibition of carboxylate inhibitors with different alkylene chain lengths on carbon steel in an alkaline solution. *RSC Adv.* 9, 7065–7077. <https://doi.org/10.1039/c8ra10083g>.
- Liu, X., Wang, J., Hu, W., 2019. Synthesis, inhibition behavior and recycling of Fe₃O₄@ZnAl-MoO₄ LDH nanocomposite inhibitor. *J. Alloy. Compd.* 801, 489–501. <https://doi.org/10.1016/j.jallcom.2019.06.118>.
- Liu, X., Gao, Y., Gao, Y., et al., 2023a. Synthesis of polyaspartic acid-glycidyl adduct and evaluation of its scale inhibition performance and corrosion inhibition capacity for Q235 steel applications. *Arab. J. Chem.* 16 <https://doi.org/10.1016/j.arabjc.2022.104515>.
- Liu, X., Gao, Y., Guan, J., et al., 2023b. Corrosion inhibition properties of spinach extract on Q235 steel in a hydrochloric acid medium. *Arab. J. Chem.* 16 <https://doi.org/10.1016/j.arabjc.2023.105066>.
- Liu, Y., Guo, X., Wang, B., et al., 2022b. Lentinan as an eco-friendly corrosion inhibitor for Q235 steel in acid medium: experimental and theoretical studies. *J. Mol. Liq.* 360 <https://doi.org/10.1016/j.molliq.2022.119513>.
- Liu, Z., Hao, X., Li, Y., et al., 2022c. Novel Ce@N-CDs as green corrosion inhibitor for metal in acidic environment. *J. Mol. Liq.* 349 <https://doi.org/10.1016/j.molliq.2021.118155>.
- Liu, Q., Wang, J., Chong, Y., et al., 2022a. Inhibition effect of green Betaine type surfactants on Q235 steel in 1 mol.L-1 hydrochloric acid: the experimental and theoretical research. *J. Mol. Struct.* 1262. <https://doi.org/10.1016/j.molstruc.2022.133023>.
- Qiang, Y., Guo, L., Li, H., et al., 2021. Fabrication of environmentally friendly Losartan potassium film for corrosion inhibition of mild steel in HCl medium. *Chem. Eng. J.* 406 <https://doi.org/10.1016/j.cej.2020.126863>.
- Qiang, Y., Ran, B., Li, M., et al., 2023. GO-functionalized MXene towards superior anti-corrosion coating. *J. Colloid Interface Sci.* 642, 595–603. <https://doi.org/10.1016/j.jcis.2023.03.167>.
- Shao, H., Yin, X., Zhang, K., et al., 2022. N-2-(3-indolyl)ethyl -cinnamide synthesized from cinnamomum cassia presl and alkaloid tryptamine as green corrosion inhibitor for Q235 steel in acidic medium. *J. Mater. Res. Technol.-Jmrt. & t.* 20, 916–933. <https://doi.org/10.1016/j.jmrt.2022.07.122>.
- Shetty, S., Rao, P., Kedimar, N., et al., 2023. Electrochemical and quantum chemical investigation to evaluate corrosion inhibition performance of therapeutic drug. *Can. Metall. Q.* <https://doi.org/10.1080/00084433.2023.2204049>.
- Wan, S., Zhang, T., Chen, H., et al., 2022. Kapok leaves extract and synergistic iodide as novel effective corrosion inhibitors for Q235 carbon steel in H₂SO₄ medium. *Ind. Crop. Prod.* 178 <https://doi.org/10.1016/j.indcrop.2022.114649>.
- Wang, L., Han, F., Zeng, G., et al., 2023a. Excellent compound inhibitor of carboxymethyl chitosan/magnetic reduced graphene oxide for carbon steel in neutral chloride solution. *Mater. Chem. Phys.* 293 <https://doi.org/10.1016/j.matchemphys.2022.126939>.
- Wang, J., Jing, J., Feng, L., et al., 2021b. Study on corrosion inhibition behavior and adsorption mechanism of novel synthetic surfactants for carbon steel in 1 M HCl solution. *Sustain. Chem. Pharm.* 23 <https://doi.org/10.1016/j.scp.2021.100500>.
- Wang, N., Liu, X., Jiang, D., 2022. Preparation of Isoetes sinensis extract as a green corrosion inhibitor for Q235 carbon steel in hydrochloric acid. *Int. J. Electrochem. Sci.* 17 <https://doi.org/10.20964/2022.12.67>.
- Wang, D.-Y., Nie, B.-L., Li, H.-J., et al., 2021a. Experimental and theoretical investigation of inhibition behavior of bisflavanol for Q235 steel in hydrochloric acid solution. *J. Mol. Liq.* 342 <https://doi.org/10.1016/j.molliq.2021.117490>.
- Wang, Y., Qiang, Y., Zhi, H., et al., 2023b. Evaluating the synergistic effect of maple leaves extract and iodide ions on corrosion inhibition of Q235 steel in H₂SO₄ solution. *J. Ind. Eng. Chem.* 117, 422–433. <https://doi.org/10.1016/j.jiec.2022.10.030>.
- Wu, Y., Guo, L., Tan, B., et al., 2021. 5-Mercapto-1-phenyltetrazole as a high-efficiency corrosion inhibitor for Q235 steel in acidic environment. *J. Mol. Liq.* 325 <https://doi.org/10.1016/j.molliq.2020.115132>.
- Wu, Y., Duan, Y., Qiu, J., et al., 2022. A pH-responsive intelligent coating based on composite CaCO₃ microspheres for long-term corrosion protection of Q235 carbon steel. *Appl. Surf. Sci.* 578 <https://doi.org/10.1016/j.apsusc.2021.151980>.
- Xing, X., Zhou, D., Tang, E., et al., 2020. A novel method to control the release rate of halloysite encapsulated Na₂MoO₄ with Ca²⁺ and corrosion resistance for Q235 steel. *Appl. Clay Sci.* 188 <https://doi.org/10.1016/j.clay.2020.105492>.
- Xiong, L., Wang, P., He, Z., et al., 2021. Corrosion behaviors of Q235 carbon steel under imidazoline derivatives as corrosion inhibitors: experimental and computational investigations. *Arab. J. Chem.* 14 <https://doi.org/10.1016/j.arabjc.2020.102952>.
- Zhang, Q.H., Hou, B.S., Li, Y.Y., et al., 2020. Two novel chitosan derivatives as high efficient eco-friendly inhibitors for the corrosion of mild steel in acidic solution. *Corros. Sci.* 164 <https://doi.org/10.1016/j.corsci.2019.108346>.
- Zhang, W., Nie, B., Wang, M., et al., 2021b. Chemically modified resveratrol as green corrosion inhibitor for Q235 steel: Electrochemical, SEM, UV and DFT studies. *J. Mol. Liq.* 343 <https://doi.org/10.1016/j.molliq.2021.117672>.
- Zhang, Y., Pan, Y., Li, P., et al., 2021c. Novel Schiff base-based cationic Gemini surfactants as corrosion inhibitors for Q235 carbon steel and printed circuit boards. *Colloids Surf. A-Physicochem. Eng. Aspects* 623. <https://doi.org/10.1016/j.colsurfa.2021.126717>.
- Zhang, R., Xiong, L., He, Z., et al., 2021a. Synthesis and structure of water-soluble sb quantum dots and enhanced corrosion inhibition performance and mechanisms. *Inorg. Chem.* 60, 16346–16356. <https://doi.org/10.1021/acs.inorgchem.1c02172>.
- Zhao, Y., Pan, T., Yu, X., et al., 2019. Corrosion inhibition efficiency of triethanolammonium dodecylbenzene sulfonate on Q235 carbon steel in simulated concrete pore solution. *Corros. Sci.* 158 <https://doi.org/10.1016/j.corsci.2019.108097>.
- Zheng, S., Feng, L., Hu, Z., et al., 2023. Study on the corrosion inhibition of biomass carbon quantum dot self-aggregation on Q235 steel in hydrochloric acid. *Arab. J. Chem.* 16 <https://doi.org/10.1016/j.arabjc.2023.104605>.
- Zheng, T., Liu, J., Wang, M., et al., 2022. Synergistic corrosion inhibition effects of quaternary ammonium salt cationic surfactants and thiourea on Q235 steel in sulfuric acid: Experimental and theoretical research. *Corros. Sci.* 199 <https://doi.org/10.1016/j.corsci.2022.110199>.
- Zhu, M., Guo, L., He, Z., et al., 2022. Insights into the newly synthesized N-doped carbon dots for Q235 steel corrosion retardation in acidizing media: a detailed multidimensional study. *J. Colloid Interface Sci.* 608, 2039–2049. <https://doi.org/10.1016/j.jcis.2021.10.160>.